



1SWASP J010313.78+352903.7: A Totally Eclipsing Binary with Components in Poor Thermal Contact

Zhijia Wang¹, Liying Zhu^{2,3}, and Kai Yuan¹

¹ School of Mathematics and Information Sciences, Yantai University, Yantai 264005, China; wzhaastro@ytu.edu.cn

² Yunnan Observatories, Chinese Academy of Sciences, Kunming 650216, China

³ School of Astronomy and Space Science, University of Chinese Academy of Sciences, Beijing 100049, China
Received 2022 September 2; revised 2022 October 17; accepted 2022 October 22; published 2022 December 9

Abstract

We presented photometry for an EB-type totally eclipsing binary, 1SWASP J010313.78+352903.7, observed with the Xinglong 85 cm telescope on 2021 October 22. Light curves in five bands (including the TESS data) were analyzed by employing the Wilson–Devinney method. The photometric solutions show that it is a contact binary with a relatively low mass ratio ($q \simeq 0.28$), relatively large fill-out factor ($f \simeq 40\%$) and large temperature difference ($\Delta T \simeq 1700$ K). Max.I–Max.II is up to about 9% of variable light amplitude of the asymmetric light curves. It is well described by double-hot spots model on the surface of the cooler secondary. The two hot spots are both in growing and evolving. They may be caused by two different mechanics, i.e., magnetic stellar activity and mass transfer. The large temperature difference between the two contact components indicates that they share a non-thermal equilibrium common envelope.

Key words: (stars:) binaries (including multiple): close – (stars:) binaries: eclipsing – stars: individual (1SWASP J010313.78+352903.7)

1. Introduction

The classic evolutionary view of close binary systems depicts the formation of contact binaries from detached binaries via magnetic angular momentum loss (AML) and shrinking of the orbit (Guinan & Bradstreet 1988; Jiang et al. 2014; Qian et al. 2018). Mass transfer through the connective channel between the two components of a contact binary will intensify or weaken the shrinkage of its orbit to some extent. These complex coupled mechanisms together with nuclear evolution will drive stellar radius and Roche lobe radius to expand or shrink. As a result the change between the two radii will feed back the rate of mass transfer and as well the evolution of the system. Recently, Yang et al. (2022) reviewed in their introduction on some key issues in the current research of contact binary. Deep, low mass ratio contact binaries are formed in the above evolutionary process and will continue to move toward merger (Yang & Qian 2015; Qian et al. 2020). Merger events though rare, like V1309 Sco (Tylenda et al. 2011; Zhu et al. 2016), yet need special concern. Researchers have investigated short period limit (Li et al. 2019; Zhang & Qian 2020) and low mass ratio limit (Li & Zhang 2006; Christopoulou et al. 2022) of contact binaries as they are highly correlated with close binary coalesce. Besides, O’Connell effect (O’Connell 1951) are common seen among late type contact binaries. By compiling nearly 700 contact binaries, Latković et al. (2021) noticed half have cool or hot spot(s). Kouzuma (2019) provided a detailed review on spots in contact

and semi-detached binaries, and pointed out that both cool spots and hot spots have different properties between W- and A-type binaries.

Apart from the asymmetric light curves, some contact systems have large depth difference in eclipse (Oh & Ahn 1992; Odell 1996; Zhu et al. 2009; Martignoni et al. 2009; Siwak et al. 2010). This means that there is a large temperature difference between their two components for these systems. They are non-thermal contact binaries (nTCBs) where the components are in poor thermal contact (Rucinski & Duerbeck 1997). Based on a statistical work of 80 nTCBs, Wang et al. (2022) noticed an evolutionary channel from strong t-ratio samples to weak t-ratio samples, during which process their common envelop will thicken. This evolutionary status has been predicted by the thermal relaxation oscillation (TRO, Lucy 1976; Flannery 1976; Robertson & Eggleton 1977) theory, whereas more issues remain obscure. To sum up, relatively-deep contact, relatively-low mass ratio, poor thermal contact and O’Connell effect are peculiar characters of contact binaries that deserve further investigation, especially for those possess most of these distinct features simultaneously.

1SWASP J010313.78+352903.7 (J0103, hereafter) = NSVS 6376701 ($\alpha_{2000} = 01:03:13.78$, $\delta_{2000} = +35:29:03.6$) was first reported in literature as a 13.02 mag star in B-band (Urban et al. 1998). Later on, based on the NSVS variables automated classification (Hoffman et al. 2009) it is classified as an EA type eclipsing binary. Its orbital period is 0.4472640 day by

Table 1
Multi-colored Photometric Observing log for J0103

Parameter	Value
Telescope	Xinglong 85 cm
Observation date	2021 October 22
Comparison star	R.A. = 01:03:45.51, decl. = +35:30:43.6
Check star	R.A. = 01:03:22.51, decl. = +35:25:51.2
Sampling	294(B) 301(V) 334(R_c) 333(I_c)
Exposure time [s]	45(B) 25(V) 20(R_c) 15(I_c)
Std. deviation($\times 10^{-2}$) [mag]	1.78(B) 1.87(V) 1.95(R_c) 1.79(I_c)
Orbital period [day]	0.44726468

referring to the Catalina surveys periodic variable catalog (Drake et al. 2014). After monitoring this target with Super-WASP for years, Lohr et al. (2015) argued that it is an EB-type eclipsing binary with an orbital period change of $-5.88(\pm 0.42) \times 10^{-7}$ day yr $^{-1}$. Sun et al. (2020) found J0103 is a contact binary with a mass ratio of 0.23 by employing an automatic Wilson–Devinney (W-D) code and photometric data collected from the Zwicky Transient Facility (ZTF) catalog.

This study sets out to investigate the photometric solutions based on data obtained from ground-based observations and space-based data. In the fourth section, we made a discussion on the reliability of physical parameters, third light, hot spot and evolutionary state of this non-thermal equilibrium contact binary system.

2. Observation

2.1. Ground-based Photometry

We monitored J0103 on 2021 October 22 with the 85 cm telescope located at the Xinglong observatory (117°575 E, 40°394 N, ~960 m), the National Astronomical Observatories, Chinese Academy of Sciences (NAOC). This prime focus telescope has a field of view of $45' \times 45'$. It is armed with an Andor CCD Camera working at 340–1000 nm covering the traditional U , B , V , R_c and I_c bands. Continuous observations to this target that covered a full phase were carried out. We used the Image Reduction and Analysis Facility (IRAF) packages to process these observed images. The observing log is tabulated in Table 1 and photometric data will be compiled to the online format soon (first 10 rows are seen in Table 2). As a result we obtained the four-color CCD photometric light curves in B , V , R_c and I_c bands. It is a totally eclipsing binary and the duration time in the secondary eclipse is about 95 minutes. The extrema of light curves for J0103 in B , V , R_c and I_c bands are figured out and listed in Table 3. It is found that Max.I–Max.II is up to about 9% of variable light amplitude of the asymmetric light curves. Such an asymmetry due to hot or cool spot caused by mass transfer or magnetic activity was also found in other contact binary systems, i.e., DZ

Psc (Yang et al. 2013), AQ Psc (Zhang et al. 2020) and V873 Per (Yang et al. 2022). After a simple modeling to the light curves during the primary eclipse we have a new linear ephemeris, Min.I (HJD) = $2459510.00157 + 0.44726468 \times E$.

2.2. TESS Time Series Light Curves

TIC 174390670 (=J0103) was observed by Transiting Exoplanet Survey Satellite (TESS) in sector 17 from 2019 October 9 to 31. In lacking short cadence observations, the long cadence (30 minutes) data were employed to conduct photometric analysis. There are two parts of light curves within sector 17 with the first 13 cycles and another 21 cycles. It is found that the phase binned light curve from the first part and the second part are completely overlapped. We then chose the first part and combined the light curves as a more compact phase binned light curve. The extrema of light curves for J0103 in the TESS band are figured out and listed in Table 3. To obtain the mid eclipse timings with TESS data, we overlapped first three cycles to one. The linear ephemeris is Min.I (BJD) = $2458766.65458 + 0.44726468 \times E$.

2.3. LAMOST Spectroscopy

The Large Sky Area Multi-Object Fiber Spectroscopic Telescope (LAMOST) as a reflecting Schmidt telescope located at the Xinglong Observatory is a “factory” in producing spectra, because it has a huge amount of fibers and catches spectra of 4000 targets simultaneously (Zhao et al. 2012). This target was observed by LAMOST on 2012 December 25 and 2014 November 14. The first measurement was taken place at 0.92 orbital phase while the second time was right at 0.5 orbital phase. The observational information is listed in Table 4. Since it is total eclipse at both zero and 0.5 phases, LAMOST captured the spectrum of the primary star at 0.5 orbital phase on the second visit (the third column of Table 4) coincidentally.

3. Photometric Solutions

Light-curves in B , V , R_c , I_c and TESS bands were performed with the W-D (Chaffee et al. 1971; Wilson 1979) code. We use the mean effective surface temperature, 7028 K, determined by LAMOST (at the second visit on 0.5 orbital phase) as the input parameter of the primary component. Gravitational-darkening coefficients were set as $g_1 = g_2 = 0.32$ (Lucy 1967), and the bolometric albedos were set as $A_1 = A_2 = 0.5$ (Ruciński 1969). Other parameters such as the inclination i , temperature of the secondary T_2 , luminosity proportions L_{1B} , L_V , L_{R_c} , L_{I_c} and L_{TESS} , and radius proportions r_{pole} , r_{side} and r_{back} are self-adaptation with the iteration of the program. During solving the light curves, we had tried to employ detached, semi-detached and contact configurations respectively. It is found that only the contact configuration (i.e., Mode 3 in W-D code) is effectual and appropriate. The key model parameter q is convergent at

Table 2
Photometric Data Observed with the Xinglong 85 cm Telescope for J0103 (first 9 rows)

HJD	Diff. Mag	HJD	Diff. Mag	HJD	Diff. Mag	HJD	Diff. Mag
+2,459,500	<i>B</i>	+2,459,500	<i>V</i>	+2,459,500	<i>R_c</i>	+2,459,500	<i>I_c</i>
9.93258	-0.211	9.93307	0.053	9.93341	0.229	9.93369	0.374
9.93417	-0.205	9.93464	0.059	9.93498	0.240	9.93527	0.395
9.93574	-0.204	9.93621	0.073	9.93656	0.238	9.93684	0.389
9.93731	-0.193	9.93779	0.070	9.93813	0.246	9.93841	0.390
9.93889	-0.179	9.93937	0.082	9.93970	0.258	9.93999	0.393
9.94046	-0.182	9.94095	0.090	9.94286	0.263	9.94156	0.405
9.94204	-0.170	9.94252	0.101	9.94444	0.278	9.94314	0.414
9.94676	-0.156	9.94410	0.106	9.94601	0.286	9.94471	0.425
9.94833	-0.149	9.94567	0.106	9.94759	0.290	9.94630	0.438
...

Table 3
The Extremum Values of Light Curves for J0103

Band	Min.I- Max.I	Min.I- Min.II	Min.I- Max.II	Max.I- Max.II	Unit
<i>B</i>	+0.572	+0.278	+0.521	-0.051	mag
<i>V</i>	+0.546	+0.252	+0.512	-0.034	mag
<i>R_c</i>	+0.535	+0.235	+0.490	-0.045	mag
<i>I_c</i>	+0.525	+0.223	+0.479	-0.046	mag
TESS band	+0.529	+0.243	+0.510	-0.020	mag

Table 4
Spectroscopic Parameters from LAMOST for J0103

Parameter	2012	2014
Obs. mid-time	HJD 2,456,286.9757	HJD 2,456,976.0237
Orbital phase	0.92	0.50
Spectral type	A9 ^a	F0
Temperature [K]	6868(±227)	7028(±20)
log <i>g</i> [dex]	4.376(±0.354)	4.151(±0.028)
[Fe/H] [dex]	4.46 (±1.87)	-0.290(±0.016)

Note.

^a Because the dispersion of the spectrum observed in 2012 is greater, this spectral type is uncertain.

0.28 and 0.29 for light curves of the 85 cm telescope and TESS, and both have minimum value of residuals. The corresponding q - Σ plot is shown in Figure 1, and the photometric solutions are tabulated in Table 5. From the table we can find that the primary star dominates the light of this system, while the third light proportion to this system is more than 15% (for the 85 cm case) and about 14% (for the TESS case). Another key parameter is the fill-out factor of 40%, which suggests a relatively-deep common envelop. Two hot spots are located on the surface of the cooler star as shown in Figure 2. The light curves with spotted and third light model are plotted in black in Figure 3. As comparison, we also provide model light curves at

the circumstance of without spot and third light plotted in red dashed curves in Figure 3. The parameters of hot spots have also been listed in the above table.

4. Results and Discussion

We carried out photometric observation for J0103 on 2021 October 22 with the Xinglong 85 cm reflecting telescope and compiled phase-folded light curves obtained from TESS database. Based on the analysis of the W-D code we found this target is a totally eclipsing and over-contact binary system. Before further conclusions are made we need to discuss on its reliability of photometric solutions previously.

4.1. Reliability of Photometric Solutions

In spite of lacking radial velocity data, our photometric solutions are yet considered relatively reliable. There are at least two specifications for this. The first is in that spectroscopic mass ratio and photometric mass ratio are coincident with each other in the cases of totally eclipsing binaries by statistical comparison (Pribulla et al. 2003; Li et al. 2021b). The orbital inclination of J0103 is close to 90° suggesting that it is a totally eclipsing binary, thus, we consider the value of mass ratio determined by analysis from photometric method a credible figure. The second reason is that this target was modeled with light curves in the *B*, *V*, *R_c*, *I_c* bands together with that of the TESS band, and they produce consistent results. Based on the above reasons, we believe that the photometric solutions and analyses to this binary system are relatively reliable. It should be pointed out that no radial velocity curves for this binary are published, thus, the absolute parameters are only estimated even if it is a totally eclipsing binary system.

4.2. Third Light

This target is not located in any crowded-field and no bright stars are found within an area of 30", meaning that the third light should probably be contributed by a close-in third star. If we suppose this third star as a main sequence star, then the

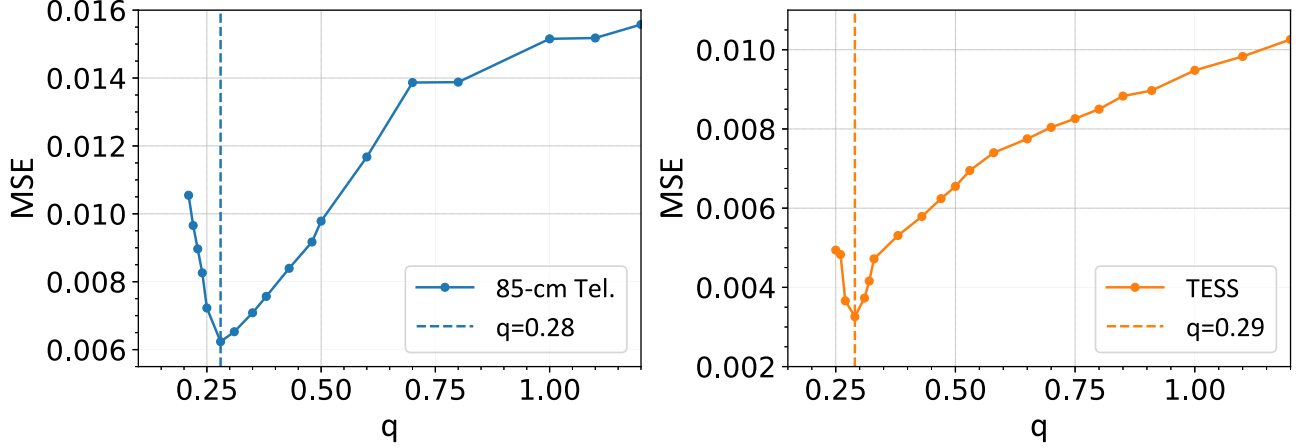


Figure 1. Searching the best globally convergent solution of mass ratio with light curve data from the Xinglong 85 cm telescope observation (left) and the TESS database (right).

Table 5
Photometric Solutions for J0103

Parameter	85 cm Telescope	TESS
type	Contact	Contact
T_1 [K] fixed	7028	7028
T_2 [K]	5374(\pm 24)	5096(\pm 19)
i [deg]	84.65(\pm 0.28)	89.25(\pm 0.25)
$q (= M_2/M_1)$	0.2806(\pm 0.0010)	0.2852(\pm 0.0024)
$L_1/(L_1 + L_2) B$	0.93899(\pm 0.00034)	...
$L_1/(L_1 + L_2) V$	0.91143(\pm 0.00057)	...
$L_1/(L_1 + L_2) R_c$	0.89404(\pm 0.00091)	...
$L_1/(L_1 + L_2) I_c$	0.8776(\pm 0.0014)	...
$L_1/(L_1 + L_2) \text{TESS}$...	0.8960(\pm 0.0010)
$L_3/L_{\text{total}} B$ (%)	18.64(\pm 0.35)	...
$L_3/L_{\text{total}} V$ (%)	17.10(\pm 0.44)	...
$L_3/L_{\text{total}} R_c$ (%)	15.56(\pm 0.63)	...
$L_3/L_{\text{total}} I_c$ (%)	15.41(\pm 0.89)	...
$L_3/L_{\text{total}} \text{TESS}$ (%)	...	13.64(\pm 0.71)
$\Omega_{1,2}$	2.3543(\pm 0.0013)	2.3498(\pm 0.0026)
fill-out factor (%)	39.03(\pm 0.72)	46.80(\pm 1.50)
r_1 (pole)	0.47602(\pm 0.00020)	0.47784(\pm 0.00042)
r_1 (side)	0.51716(\pm 0.00028)	0.51992(\pm 0.00061)
r_1 (back)	0.54717(\pm 0.00040)	0.55135(\pm 0.00094)
r_2 (pole)	0.2723(\pm 0.0011)	0.2771(\pm 0.0025)
r_2 (side)	0.2859(\pm 0.0014)	0.2916(\pm 0.0032)
r_2 (back)	0.3340(\pm 0.0031)	0.3443(\pm 0.0077)
Hot Spot 1		
θ [rad]	6.17347	6.15999
ϕ [rad]	1.57467	1.57467
r_s/r_*	0.63979	0.74876
T_s/T_*	1.31921	1.36987
Hot Spot 2		
θ [rad]	1.24259	1.22635
ϕ [rad]	1.39253	1.49913
r_s/r_*	0.72164	0.62910
T_s/T_*	1.20382	1.21465
residuals	0.00484	0.00239

mass is estimated as of $M_3 = 1.13_{-0.01}^{+0.01} M_\odot$ (see in Section 4.4). One of the future works is suggested to focus on the cyclic change of orbital period and the potential hierarchical third star to this eclipsing binary system.

4.3. Hot Spot

Hot spot events are seen in many contact binaries, i.e. KQ Gem (Zhang 2010), DZ Psc (Yang et al. 2013), J004505 (Li et al. 2022) etc. They are believed to be caused by magnetic stellar activity or mass transfer impact (Lee et al. 2009, 2010). As in the case of J0103 two hot spots are found on the surface of the secondary component. One is covering the contact part of its Roche lobe (Hot Spot 1) and the other is on its side (Hot Spot 2). Hot Spot 1 is suggested to be the result of undercurrent from the hotter star to the cooler star. The hot gas stream impact the cooler component and warmed up the local region (i.e., Hot Spot 1). Such a phenomenon has also been found in other individual cases (Latković & Čeki 2021), while the second hot spot (Hot Spot 2) may be the result of magnetic stellar activity. Moreover, we noticed that Hot Spot 1 had shrunk slightly from BJD 2,458,769 to HJD 2,459,510 within 2 yr, revealing that the rate of mass transfer was decreasing. The scale of the second hot spot (Hot Spot 2) had grown slightly larger. It may implies that the magnetic activity in this region was enhancing.

4.4. Absolute Physical Parameters

Observational result of LAMOST at the 0.50 orbital phase suggests that the spectral type of the primary star of J0103 is F0. By referring to Cox (2000), the mass of the primary should be $M_1 = 1.60_{-0.04}^{+0.08} M_\odot$. The errors come from interval of adjacent spectral type. From the piecewise empirical mass–luminosity relations (Eker et al. 2018), we can estimate the

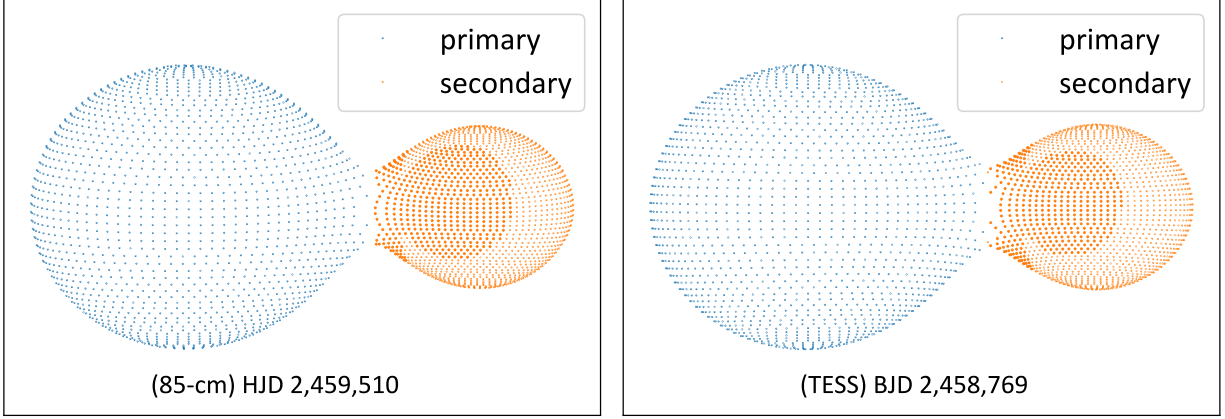


Figure 2. The 3D configurations of J0103 at 0.25 orbital phase.

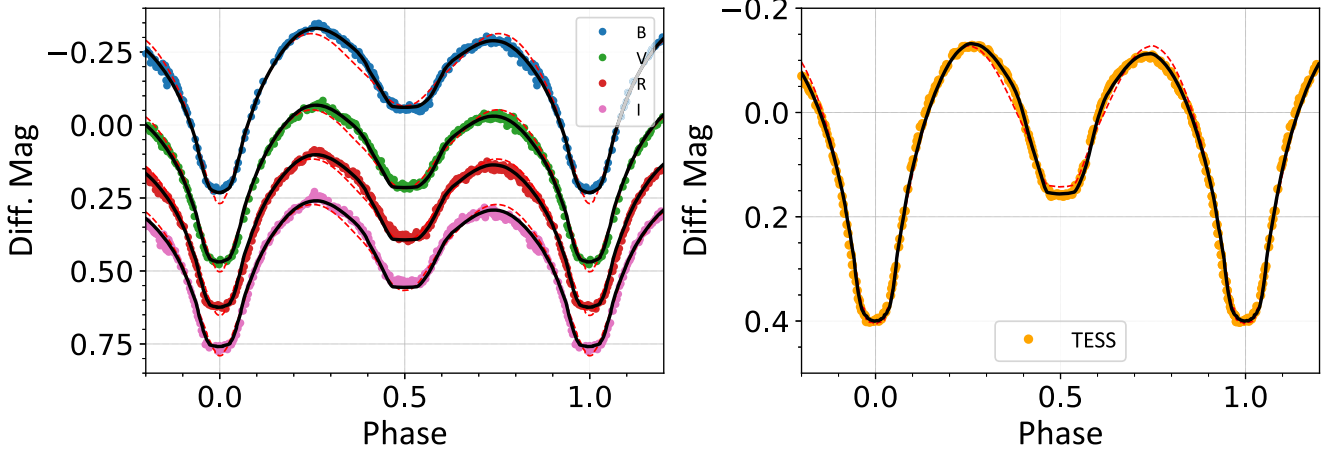


Figure 3. Comparing observational light curves and model ones. The Xinglong 85 cm telescope observations (left) and the TESS case (right).

luminosity of the primary star as of $7.83^{+0.10}_{-0.05} L_{\odot}$. As mass ratio is determined as of 0.28, the mass of the secondary star is estimated as $0.45^{+0.02}_{-0.01} M_{\odot}$. By employing the simplified Kepler's third law, $(M_1 + M_2)P^2 = 0.0134a^3$, and values of relative radius in Table 5, we can obtain the separation, $a = 3.12^{+0.05}_{-0.03} R_{\odot}$, and the absolute radii, $R_1 = 1.60^{+0.03}_{-0.01} R_{\odot}$ and $R_2 = 0.93^{+0.01}_{-0.01} R_{\odot}$. The luminosity of the secondary component is estimated as $0.76^{+0.10}_{-0.04} L_{\odot}$. Also, the luminosity of the third light is estimated as of $1.76^{+0.04}_{-0.02} L_{\odot}$. If we suppose the origin of this additional light comes from a main sequence close-in third star, then the mass and radius should be $1.13^{+0.01}_{-0.01} M_{\odot}$ and $1.18^{+0.01}_{-0.01} R_{\odot}$ by referring to the piecewise empirical relations (Eker et al. 2018). The physical parameters are listed in Table 6, from which we can draw the primary (blue dot) and secondary (red dot) components on the Hertzsprung-Russell diagram (HR; Figure 4). They are both located within the main sequence region.

Table 6
Absolute Parameters for the J0103 Binary System

Parameter	Value	Unit
M_1	$1.60^{+0.08}_{-0.04}$	M_{\odot}
M_2	$0.45^{+0.02}_{-0.01}$	M_{\odot}
R_1	$1.60^{+0.03}_{-0.01}$	R_{\odot}
R_2	$0.93^{+0.01}_{-0.01}$	R_{\odot}
L_1	$7.83^{+0.10}_{-0.05}$	L_{\odot}
L_2	$0.76^{+0.10}_{-0.04}$	L_{\odot}
a	$3.12^{+0.05}_{-0.03}$	R_{\odot}
M_3^a	$1.13^{+0.01}_{-0.01}$	M_{\odot}
R_3^a	$1.18^{+0.01}_{-0.01}$	R_{\odot}
L_3^a	$1.76^{+0.04}_{-0.02}$	L_{\odot}

Note.

^a These parameters come from the assumed additional main sequence star.

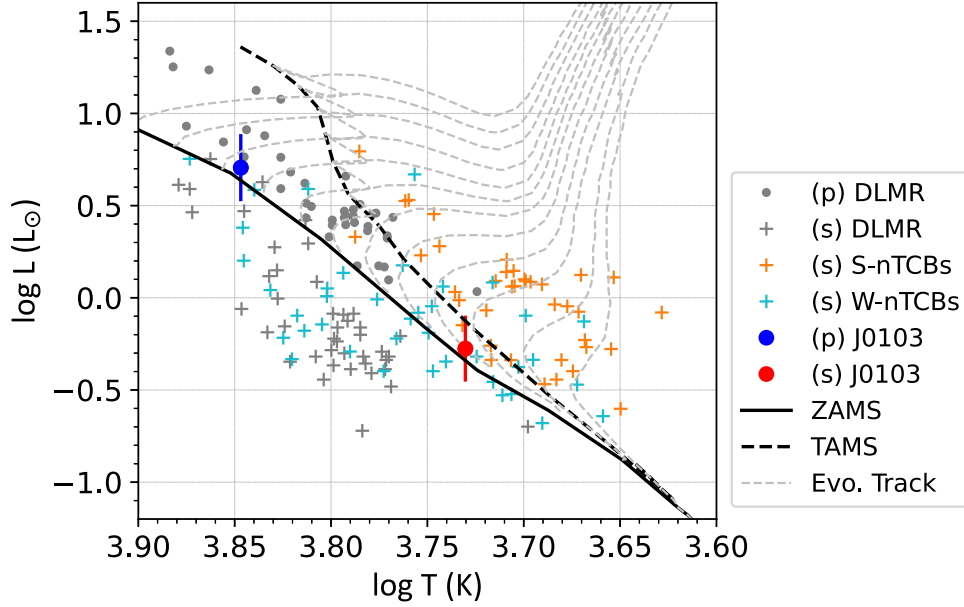


Figure 4. HR diagram with zero age main sequence, terminal age main sequence obtained from Bressan et al. (2012). The blue and red dots with err bars are the primary and secondary component of J0103. The background gray dots and gray crosses represent the primary and secondary components of deep low mass ratio (DLMR) over-contact binaries taken from Yang & Qian (2015); the orange and cyan crosses stand for secondary components of STRONG t -ratio and WEAK t -ratio non-thermal contact binaries (nTCBs) are taken from Table A2 in Wang et al. (2022), where the STRONG t -ratio samples to those with relative temperature difference (t -ratio), $(T_1 - T_2)/T_1 > 0.2$ and the WEAK t -ratio samples to those $0.05 < t$ -ratio = $(T_1 - T_2)/T_1 < 0.2$.

4.5. Evolutionary Property

Figure 4 shows the HR diagram. We collected samples of deep low mass ratio (DLMR) over-contact binaries from Yang & Qian (2015), where the gray dots and gray crosses represent the primary and secondary components respectively. The orange and cyan crosses stand for secondary components of STRONG t -ratio and WEAK t -ratio non-thermal equilibrium contact binaries (nTCBs) are taken from Wang et al. (2022), which pointed that the STRONG t -ratio samples will evolve to WEAK t -ratio samples through heat and mass transfer along with angular momentum loss, meanwhile thickening their common envelop. Also we find in Figure 4 that there is a tendency that WEAK t -ratio nTCBs are evolving toward DLMR over-contact binaries if thermal equilibrium is continuously establishing. As a result that the secondary components have been away from the main sequence. This is not the case as the temperature determined to the secondary components are just that of the common envelop.

After the analysis of the obtained light curves in the B , V , R_c and I_c bands and that of the TESS band we found that J0103 is an over-contact binary having a lower mass ratio ($q = 0.28$). Though it has a relatively-deep common envelope for the fill-out factor is 40%, its surface temperature difference between the two components is however as high as of 1700 K. It indicates that this target is undergoing a non-thermal equilibrium contact evolutionary state. This is in agreement

with the theory of thermal relaxation oscillations (TRO) proposed by several researchers (Flannery 1976; Lucy 1976; Robertson & Eggleton 1977). By the analysis of 27 hot contact binaries, Qian (2001) found that the evolution of hot W UMA stars are mainly dominated by TRO rather than weak influence by angular momentum loss; whereas the evolution of the cooler ones are dominated by both mechanisms. Also the combination of TRO and angular momentum loss can explain the physical parameter distributions of over contact binaries (Qian 2003). Another hypothesis is that J0103 is undergoing an unstable and intermittent mass transfer from the primary to the secondary. During this process the Roche lobe will instantaneously shrink, and present a restoring and delaying thick envelop. J0103 is therefore on the key evolutionary stage of warming the common envelop of the cooler side. Though we are not clear of the physics of its current relatively-deep contact configuration, this system will gradually establish thermal equilibrium common envelop and will thicken it to some extend.

As investigated by Li & Zhang (2006), Yang & Qian (2015), Kim et al. (2019), Li et al. (2021a) and Christopoulou et al. (2022), low mass ratio deep contact binaries have a relationship between $J_{\text{spin}}/J_{\text{orb}}$ and q . To better understand the character of samples with large temperature difference between two components, we also revisited samples of nTCBs from Wang et al. (2022) and figured out their $J_{\text{spin}}/J_{\text{orb}}$ at $k^2 = 0.05$. We constructed the $q - J_{\text{spin}}/J_{\text{orb}}$ diagram and discriminated the unstable region and stable region of contact binaries by the

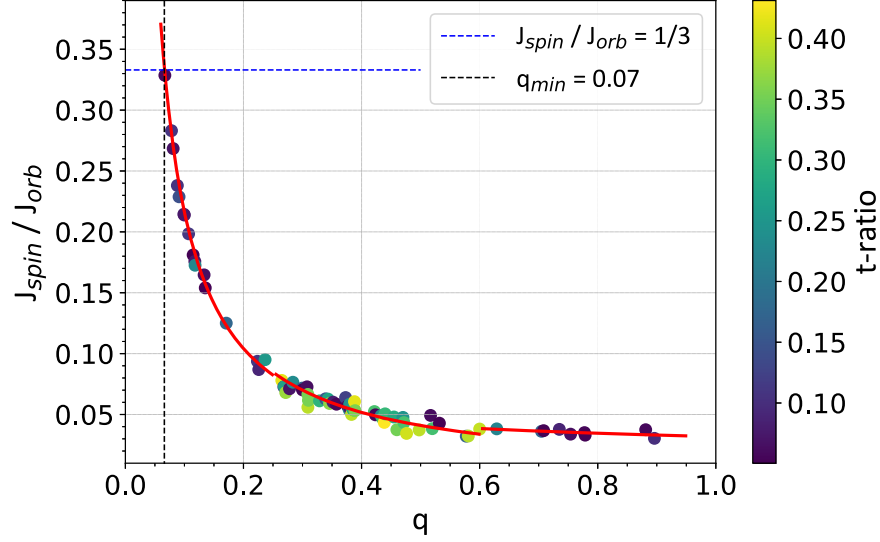


Figure 5. Relations of $q - J_{spin}/J_{orb}$ at $k^2 = 0.05$. Dots are nTCBs taken from Wang et al. (2022). The red solid lines are plotted using Equations (1), (2) and (3). The blue dashed line is the boundary of unstable and stable contact systems; the black dashed line marks the lower limit of mass ratio.

boundary of $J_{orb} = 3J_{spin}$ (blue dashed line in Figure 5). From the figure we can find that STRONG t -ratio samples are mostly distributed between the q value of 0.25 and 0.6, whereas the WEAK t -ratio samples are located mostly in both sides. Three piecewise regression models are adopted to produce best fitting (red solid lines in Figure 5). The fitting curves are

$$\begin{aligned} \log \frac{J_{spin}}{J_{orb}} &= -1.050(\pm 0.018)(\log q) - 1.719(\pm 0.015), \\ r &= -0.9965, \quad (0.05 < q < 0.25), \end{aligned} \quad (1)$$

$$\begin{aligned} \log \frac{J_{spin}}{J_{orb}} &= -1.049(\pm 0.086)(\log q) - 1.704(\pm 0.034), \\ r &= -0.8987, \quad (0.25 < q < 0.60), \end{aligned} \quad (2)$$

$$\begin{aligned} \log \frac{J_{spin}}{J_{orb}} &= -0.372(\pm 0.157)(\log q) - 1.497(\pm 0.022), \\ r &= -0.6421, \quad (0.60 < q < 0.90). \end{aligned} \quad (3)$$

As a result that a mass ratio cut-off at $q = 0.07$ (black dashed line in Figure 5) was derived. It predicts that no nTCBs could be observed with mass ratio lower than this limitation.

5. Summary

Discovery and investigation of a unique individual contact binary 1SWASP J010313.78+352903.7 allowed us to better understand the diversity of contact binary zoo. To the best of our knowledge, J0103 possesses at least five major and distinct features simultaneously:

1. Total eclipse, for the orbital inclination is 85° .
2. Relatively-deep contact binary, where the fill-out factor is about 40% or more.

3. Relatively-low mass ratio, where $q = 0.28$ is at the boundary between very low mass ratio samples and intermediate ones.
4. Poor thermal contact, where the temperature difference between the two components is 1700 K.
5. O'Connell effect and hot spot. There are two hot spots on the secondary star which have caused the asymmetry of light curves between the two maxima (O'Connell effect).

As a natural astrophysical laboratory, such a population has continually fascinated us in many aspects. Future efforts are deserved to concentrate on more such peculiar targets.

Acknowledgments

We appreciate the constructive remarks and suggestions provided by the anonymous referee. This work is supported by the Natural Science Foundation of Shandong Province, China (ZR2021QA082), the National Natural Science Foundation of China (No. 11922306) and the Doctoral Start-up Foundation of Yantai University (SX20B112). We acknowledge the support of the staffs of the Xinglong 85 cm telescope, NAOC, CAS, China. In addition, the Guo Shou Jing Telescope (the Large Sky Area Multi-Object Fiber Spectroscopic Telescope LAMOST) is a National Scientific Project built by the Chinese Academy of Sciences. Funding for the project has been provided by the National Development and Reform Commission. LAMOST is operated and managed by the National Astronomical Observatories, Chinese Academy of Sciences. This paper includes data collected with the TESS mission, obtained from the MAST data archive at the Space Telescope

Science Institute (STScI); and data obtained from the European Space Agency (ESA) space mission Gaia.

References

- Bressan, A., Marigo, P., Girardi, L., et al. 2012, *MNRAS*, 427, 127
- Chaffee, F. H. J., Carbon, D. F., & Strom, S. E. 1971, *ApJ*, 166, 593
- Christopoulou, P.-E., Lalounta, E., Papageorgiou, A., et al. 2022, *MNRAS*, 512, 1244
- Cox, A. N. 2000, *Allen's Astrophysical Quantities* (Berlin: Springer)
- Drake, A. J., Graham, M. J., Djorgovski, S. G., et al. 2014, *ApJS*, 213, 9
- Eker, Z., Bakış, V., Bilir, S., et al. 2018, *MNRAS*, 479, 5491
- Flannery, B. P. 1976, *ApJ*, 205, 217
- Guinan, E. F., & Bradstreet, D. H. 1988, in *NATO Advanced Study Institute (ASI) Series C, Formation and Evolution of Low Mass Stars*, Vol. 241 ed. A. K. Dupree & M. T. V. T. Lago, 345
- Hoffman, D. I., Harrison, T. E., & McNamara, B. J. 2009, *AJ*, 138, 466
- Jiang, D., Han, Z., & Li, L. 2014, *MNRAS*, 438, 859
- Kim, C.-H., Song, M.-H., Park, J.-H., et al. 2019, *JASS*, 36, 265
- Kouzuma, S. 2019, *PASJ*, 71, 21
- Latković, O., & Čeki, A. 2021, *PASJ*, 73, 132
- Latković, O., Čeki, A., & Lazarević, S. 2021, *ApJS*, 254, 10
- Lee, J. W., Youn, J.-H., Han, W., et al. 2010, *AJ*, 139, 898
- Lee, J. W., Youn, J.-H., Lee, C.-U., Kim, S.-L., & Koch, R. H. 2009, *AJ*, 138, 478
- Li, F. X., Qian, S. B., Jiao, C. L., & Ma, W. W. 2022, *ApJ*, 932, 14
- Li, K., Xia, Q.-Q., Kim, C.-H., et al. 2021a, *ApJ*, 922, 122
- Li, K., Xia, Q.-Q., Michel, R., et al. 2019, *MNRAS*, 485, 4588
- Li, K., Xia, Q.-Q., Kim, C.-H., et al. 2021b, *AJ*, 162, 13
- Li, L., & Zhang, F. 2006, *MNRAS*, 369, 2001
- Lohr, M. E., Norton, A. J., Payne, S. G., West, R. G., & Wheatley, P. J. 2015, *A&A*, 578, A136
- Lucy, L. B. 1967, *ZAp*, 65, 89
- Lucy, L. B. 1976, *ApJ*, 205, 208
- Martignoni, M., Acerbi, F., & Barani, C. 2009, *RAA*, 9, 1270
- O'Connell, D. J. K. 1951, *PRCO*, 2, 85
- Odell, A. P. 1996, *MNRAS*, 282, 373
- Oh, K.-D., & Ahn, Y.-S. 1992, *Ap&SS*, 187, 261
- Pribulla, T., Kreiner, J. M., & Tremko, J. 2003, *CoSka*, 33, 38
- Qian, S. 2001, *MNRAS*, 328, 914
- Qian, S. 2003, *MNRAS*, 342, 1260
- Qian, S. B., Zhang, J., He, J. J., et al. 2018, *ApJS*, 235, 5
- Qian, S.-B., Zhu, L.-Y., Liu, L., et al. 2020, *RAA*, 20, 163
- Robertson, J. A., & Eggleton, P. P. 1977, *MNRAS*, 179, 359
- Ruciński, S. M. 1969, *AcA*, 19, 245
- Rucinski, S. M., & Duerbeck, H. W. 1997, *PASP*, 109, 1340
- Siwak, M., Zola, S., & Koziel-Wierzbowska, D. 2010, *AcA*, 60, 305
- Sun, W., Chen, X., Deng, L., & de Grijs, R. 2020, *ApJS*, 247, 50
- Tylenda, R., Hajduk, M., Kamiński, T., et al. 2011, *A&A*, 528, A114
- Urban, S. E., Corbin, T. E., Wycoff, G. L., et al. 1998, *AJ*, 115, 1212
- Wang, Z. H., Zhu, L. Y., & Yuan, K. 2022, *MNRAS*, 517, 1007
- Wilson, R. E. 1979, *ApJ*, 234, 1054
- Yang, Y.-G., & Qian, S.-B. 2015, *AJ*, 150, 69
- Yang, Y. G., Qian, S. B., Zhang, L. Y., Dai, H. F., & Soonthornthum, B. 2013, *AJ*, 146, 35
- Yang, Y., Yuan, H., Wang, S., & Dai, H. 2022, *AJ*, 163, 250
- Zhang, L.-y 2010, *PASP*, 122, 309
- Zhang, L., Zhu, Z., Yue, Q., et al. 2020, *MNRAS*, 491, 6065
- Zhang, X.-D., & Qian, S.-B. 2020, *MNRAS*, 497, 3493
- Zhao, G., Zhao, Y.-H., Chu, Y.-Q., Jing, Y.-P., & Deng, L.-C. 2012, *RAA*, 12, 723
- Zhu, L. Y., Qian, S. B., Zola, S., & Kreiner, J. M. 2009, *AJ*, 137, 3574
- Zhu, L.-Y., Zhao, E.-G., & Zhou, X. 2016, *RAA*, 16, 68